

Interpreting seasonal convective mixing in Devils Hole, Death Valley National Park, from temperature profiles observed by fiber-optic distributed temperature sensing

Mark B. Hausner,¹ Kevin P. Wilson,² D. Bailey Gaines,² and Scott W. Tyler¹

Received 27 May 2011; revised 20 March 2012; accepted 21 March 2012; published 8 May 2012.

[1] Devils Hole, a groundwater-filled fracture in the carbonate aquifer of the southern Nevada Mojave Desert, represents a unique ecohydrological setting, as home to the only extant population of *Cyprinodon diabolis*, the endangered Devils Hole pupfish. Using water column temperatures collected with a fiber-optic distributed temperature sensor (DTS) during four field campaigns in 2009, evidence of deep circulation and nutrient export are, for the first time, documented. The DTS was deployed to measure vertical temperature profiles in the system, and the raw data returned were postprocessed to refine the calibration beyond the precision of the instrument's native calibration routines. Calibrated temperature data serve as a tracer for water movement and reveal a seasonal pattern of convective mixing that is supported by numerical simulations of the system. The periodic presence of divers in the water is considered, and their impacts on the temperature profiles are examined and found to be minimal. The seasonal mixing cycle may deplete the pupfish's food supplies when nutrients are at their scarcest. The spatial and temporal scales of the DTS observations make it possible to observe temperature gradients on the order of $0.001^{\circ}\text{C m}^{-1}$, revealing phenomena that would have been lost in instrument noise and uncertainty.

Citation: Hausner, M. B., K. P. Wilson, D. B. Gaines, and S. W. Tyler (2012), Interpreting seasonal convective mixing in Devils Hole, Death Valley National Park, from temperature profiles observed by fiber-optic distributed temperature sensing, *Water Resour. Res.*, *48*, W05513, doi:10.1029/2011WR010972.

1. Introduction

[2] Devils Hole ($36^{\circ}25'N$, $116^{\circ}17'W$) is a geothermal pool in the carbonate aquifer of the southern Nevada Mojave Desert. Despite its small surface area (the water surface of Devils Hole is $<60\text{ m}^2$), Devils Hole reaches depths of more than 130 m, and the system is home to the entire population of the endangered Devils Hole pupfish (*Cyprinodon diabolis*). The combination of hydrologic, geologic, and ecological factors at work in Devils Hole has made it a focus of international research spanning decades. Devils Hole has provided the backdrop for seminal work in ichthyology [Chernoff, 1985], evolution [Miller, 1950; Lema and Nevitt, 2006; Meffe, 1986], palaeoclimate reconstruction [Szabo et al., 1994; Winograd et al., 2006], and most recently, one of the sharpest intersections of ecology and hydrology. Legal decisions governing Devils Hole and *C. diabolis* have helped shaped the way the United States manages environments for the preservation of endangered species; the 1976 U.S. Supreme Court decision in *Cappaert versus United States* set a precedent for resource management on federally protected lands, holding that reservation of land for the purposes of maintaining a species

implied simultaneous reservation of the resources (in this case, water rights) required for that maintenance. At the same time, the depth of Devils Hole and the connection to the Death Valley regional flow system offers a unique opportunity to examine the complex interactions between surface pools and the carbonate aquifer.

[3] Devils Hole itself and the 16 hectare parcel surrounding it are located within the bounds of Ash Meadows National Wildlife Refuge, but managed as a disjunct unit of Death Valley National Park [Anderson and Deacon, 2001]. There is no surface outlet for the water, and the spring is fed by groundwater flowing through the carbonate aquifer underlying the Ash Meadows area. Listed in 1967 by the U.S. Fish and Wildlife Service as an endangered species [Anderson and Deacon, 2001], the Devils Hole pupfish population has varied over the last 40 yr from peaks near 600 individuals to low counts of fewer than 40 fish. The population has always varied seasonally, with autumn highs and spring lows [Anderson and Deacon, 2001], and is currently stable at ~ 100 individuals. When groundwater pumping came online as an irrigation source in the early 1960s, the water level in Devils Hole began a precipitous decline and the pupfish population soon followed suit. *Cappaert versus United States* (1976) led to a halt in groundwater withdrawals in the area, and the recovery of the pupfish population tracked the recovery of the water level until the water table stabilized in the early 1980s [Anderson and Deacon, 2001]. Beginning in 1995, however, the pupfish population again began to decline [Riggs and Deacon,

¹Department of Geologic Sciences and Engineering, University of Nevada, Reno, Nevada, USA.

²Death Valley National Park, Pahrump, Nevada, USA.

2002]. This drop was not tied to the water level in Devils Hole, and the reason for the population decline is still not understood. A number of the hypotheses advanced to explain the recent decline in the pupfish population posit changes to the physical habitat of the system [Riggs and Deacon, 2002; Threlloff and Manning, 2003].

[4] The physical habitat of the Devils Hole pupfish comprises a number of factors beyond water level. Water temperatures are particularly important to the population as the waters of Devils Hole are nearly always between 33°C and 34°C, near the upper tolerance of most *Cyprinodon* species. Water temperatures strongly influence the viability of *Cyprinodon* eggs and larvae [Lema and Nevitt, 2006], and the pupfish population is thought to be particularly sensitive to temperatures on the shallow shelf that occupies the southern 6.3 m of the system [Threlloff and Manning, 2003]. This shallow shelf contains the most suitable habitat for spawning, and also provides substrate for the benthic community; fish use the shelf on a daily basis to forage and spawn, although these behaviors also occur below the shallow shelf. In addition to temperatures in both the water column and the substrate, the availability of food also impacts the pupfish population. The pupfish diet varies seasonally over the course of the year, driven primarily by the variations in the direct insolation falling on the water surface and the resulting cycles in primary production. During the summer, when primary productivity is at an annual peak, the pupfish diet is driven primarily by *Oscillatoria* and *Plectonema* (both filamentous cyanobacteria) and *Spirogyra* (a filamentous green algae) that grow on the substrate in the shallow shelf [Wilson and Blinn, 2007]. At the same time, allochthonous carbon inputs reach an annual peak, with 35% of the annual allochthonous carbon input entering the system in June and July [Wilson and Blinn, 2007]. When the exposure to the sun is limited by the high canyon walls, however, these food sources are not as available. Wilson and Blinn [2007] found that the food-limited winter diet of the pupfish consisted primarily of the riffle beetle (*Stenelmis calida*, which made up 50.5% of the diet) and a scavenging flatworm (*Dugesia dorotocephala*, 35.8% of the diet). Although solar radiation influences primary productivity, productivity rates are also controlled by water temperatures and the availability of nitrogen and phosphorus required by algae. Both water temperatures [Threlloff and Manning, 2003] and nutrient concentrations exhibit seasonal variations [Wilson and Blinn, 2007] on the shallow shelf.

[5] In most temperate lakes, water temperatures and nutrient cycling are strongly affected by seasonal convective mixing (i.e., turnover), which occurs when water on the surface cools until the density is great enough to plunge into the underlying waters. The sinking water displaces water from near the bottom, and the water column effectively “turns over,” carrying suspended material and dissolved oxygen from the epilimnion (the warmer waters of the lake above the thermocline) to the lake bottom and bringing hypoxic water, reduced nutrients, and settled detritus back up from the depths. The changes in temperature and redox chemistry caused by convective mixing are critical drivers of many lake ecosystems. Hydrogeologic settings, in which the geothermal gradient allows for the transfer of heat from deeper in the system upward to the surface, behave differently. In porous media, thermal

gradients can be considered as part of a total potential gradient [Bear and Cheng, 2010], and thermal convection is controlled by the potential gradient, media grain and pore size, and the intrinsic permeability of the media [Bejan, 2003]. In the carbonate aquifer underlying Ash Meadows, the vertical geothermal gradient is $\sim 7^\circ\text{C km}^{-1}$ [Reiner, 2007], and the fractured aquifer complicates our understanding of saturated flow [Faunt et al., 2004]. Just as Devils Hole itself is a mixture of surface waters and groundwater, the mixing processes at work in the deep pool of Devils Hole are a combination of those seen in limnological settings and groundwater settings. The processes controlling temperature and nutrient availability in Devils Hole depend on its unique structure and relationship to the carbonate aquifer underlying Ash Meadows.

[6] In 2009, a fiber-optic distributed temperature sensor (DTS) was employed to periodically measure vertical temperature profiles in Devils Hole, and data collected over the course of four 2–4 d field deployments point toward a pattern of seasonal convective mixing. Because of the high heat capacity and low thermal diffusivity of water, changes in water temperature may indicate groundwater fluxes [Anderson, 2005] or hyporheic exchange [Selker et al., 2006], and fast temperature changes in fluid systems may be used as an indicator of convective mixing [Suárez et al., 2010]. With the introduction of DTS for hydrologic research applications, it is now possible to observe temperature at spatial and temporal scales that were once prohibitively expensive or impractical to achieve [Tyler et al., 2009]. At Devils Hole, a series of individually calibrated temperature sensors at discrete depths (every 5 m, for example) would not have shown the seasonal signals discussed in this paper; the use of a DTS to record a set of spatially distributed temperature observations with a single common calibration helps to resolve very small temperature differences (on the order of hundredths to tenths of a degree centigrade) and to observe phenomena that may have been lost in the noise of more traditional measurement techniques. This paper presents a novel model of seasonal convection in the deep pool of Devils Hole based on high-precision temperature profiles observed with a DTS and discusses impacts of that convection on this unique ecological and hydrological community and its implications toward management of the ecosystem of the endangered pupfish.

2. Study Site, Materials, and Methods

[7] This section describes the physical setting of Devils Hole, as well as the data collection, calibration, statistical, and modeling methods employed in this study. Data were collected using a fiber-optic DTS instrument, calibrated with independent temperature measurements in water baths. Methods used include statistical analyses, numerical simulations using a commercially available computational fluid dynamics (CFD) software package, and flow characterization with dimensionless numbers.

2.1. Devils Hole System

[8] Devils Hole (Figure 1) is composed of an open fault in the limestone bedrock, with a free water surface ~ 17 m below grade and an aperture that extends to a depth of at

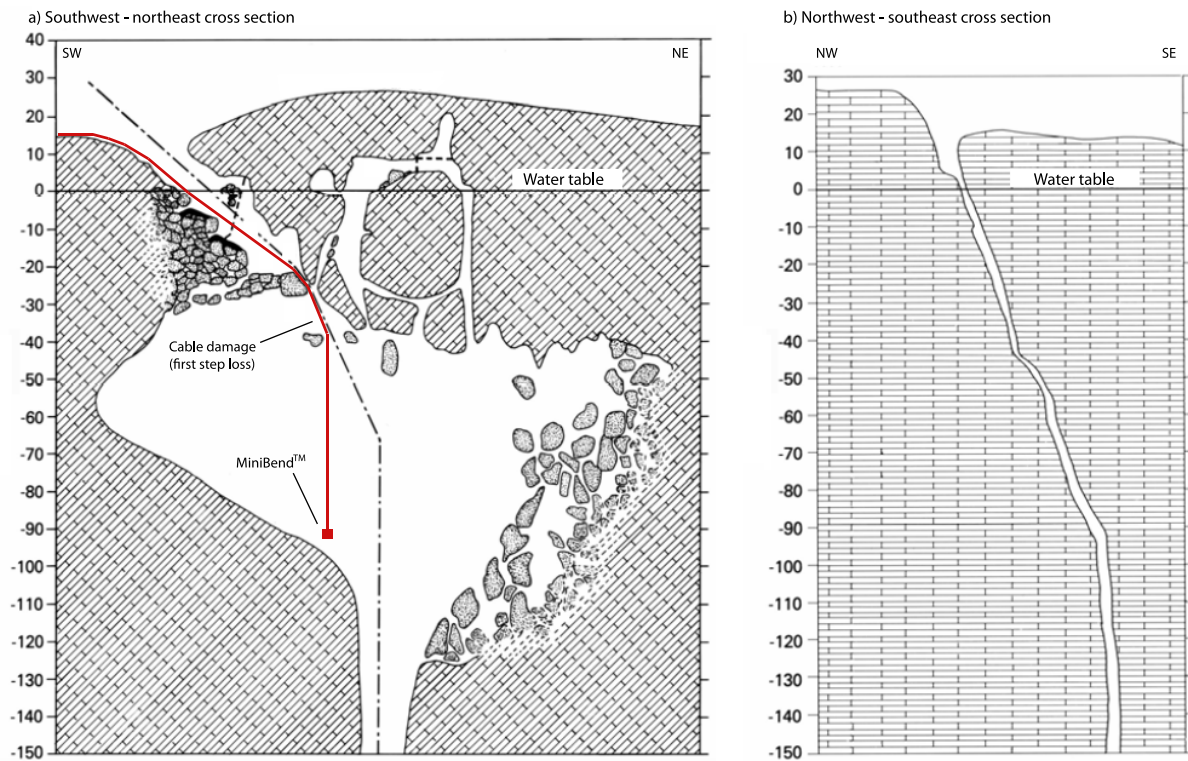


Figure 1. (a) Southwest-northeast and (b) northwest-southeast orthogonal cross-sections of Devils Hole as sketched by frequent Devils Hole diver A.C. Riggs [after Riggs and Deacon, 2002]. The placement of the fiber-optic cable is shown in red on (a). Because of signal losses in the fiber-optic cable, the useful data are limited to those collected at less than 34 m deep, near the constriction above the large cavern as indicated on (a). In both (a) and (b), the horizontal scale is the same as the vertical scale.

least 130 m below the water surface [Szabo *et al.*, 1994]. Although nearby groundwater pumping was stopped in 1977, the water level in Devils Hole shows significant variation; earth tide effects drive a semidiurnal variation of up to 12 cm [Riggs and Deacon, 2002]. There are two distinct features to the system: a shallow shelf ($\sim 2.6 \text{ m} \times 6.3 \text{ m}$, with a water depth ranging from 5 to 70 cm), and the deep pool of unknown depth to the north of the shelf ($\sim 3 \text{ m} \times 10 \text{ m}$ on the surface) [Riggs and Deacon, 2002].

[9] The fracture that forms the deep pool of Devils Hole is $\sim 4 \text{ m}$ wide along the NW-SE axis for the entire known depth, but the system opens into a cavernous room on the NE-SW axis below a depth of 30 m. This cavern is roughly 50 m wide, and samples taken from depths of 8–45 m show ultraoligotrophic water [D. P. Moser, Desert Research Institute, Las Vegas, NV, personal communication, 2010]. In the upper 22 m of the system, dissolved oxygen concentrations are a fairly uniform $2.5\text{--}3 \text{ mg l}^{-1}$ [Baugh and Deacon, 1983]; data on deeper oxygen concentrations are not available. Water temperatures 5 m below the shallow shelf range from 33.5°C to 34°C , and show little or no diurnal variation [Threlloff and Manning, 2003]. While the full depth of Devils Hole is unknown, divers have descended as far as 133 m, and the clarity of the water allowed a view to $\sim 150 \text{ m}$, where the steep angle of the fracture obstructed their sightlines [Riggs and Deacon, 2002]. Water chemistry in the deep pool is remarkably consistent, with pH and

specific conductance varying less than 1% from the mean over the course of a year in the upper 4–5 m of the pool profile [Wilson and Blinn, 2007]. Nutrient concentrations, however, do change, with orthophosphate, nitrate, and ammonia exhibiting significant variation over the course of the year [Wilson and Blinn, 2007].

[10] The shelf is actually a boulder perched between the two walls of the fracture, and is oriented along the north-east-southwest axis and in communication at the north end with the deep pool. The south end of the shelf is generally shallower, with the water depth increasing toward the north end of the deep pool; the rounded northern edge of the boulder forms a transition zone, dropping away to form a “ramp” down which cooler water can flow into the deep pool. Typical water temperatures on the shelf range from 32°C to 36°C , depending on the season, but nighttime temperatures can drop to 30°C or less when the timing of low tide coincides with cool winter nights [Threlloff and Manning, 2003].

2.2. Fiber-Optic Distributed Temperature Sensing

[11] Vertically distributed temperature data were collected in the upper part of the deep pool of Devils Hole using a Sensornet Sentinel DTS (Sensornet LTD, Hertfordshire, England) and a BruSteel fiber-optic cable (Brugg Kabel, Brugg, Switzerland). The 235-m long cable is composed of a steel capillary tube containing two duplexed fibers that are spliced together with a MiniBend (AFL

Telecommunications, Duncan, South Carolina) at the submerged end of the cable. A twisted wire sleeve surrounding the capillary tube provides additional tensile strength, and a PVC jacket insulates and protects the cable itself. The cable was installed by the Devils Hole Dive Team in January 2009, and has been in place since that installation. The placement of the cable is indicated by the red line in Figure 1a. The cable is anchored at the top of the east ridge overlooking Devils Hole, and is interrogated using a DTS temporarily positioned above this ridge. A second anchor ~ 1 m above the water surface provides strain relief for the cable and secures it in a constant location, and a weight at the bottom of the cable keeps tension on it in the water column.

[12] A 25-m coil of cable with a 100 Ω platinum resistance temperature detector (PT100 RTD) (Sensonet LTD) was placed in a calibration water bath at the surface, and a 15-m coil of cable with a second PT100 RTD (Thermoworks Inc., Lindon, Utah) was secured horizontally in situ, ~ 15 cm below the water surface in Devils Hole. The in situ reference coil was installed below an existing instrument to minimize the effects of solar radiation, and the horizontal orientation minimized the impacts of vertical stratification. Each of the PT100 sensors was calibrated against a NIST-traceable thermometer ($\pm 0.05^\circ\text{C}$; Control Company, Friendswood, TX) prior to installation. The calibration coils serve to maintain reference sections of the cable, where a known length of cable is kept at a known temperature for calibration of the DTS temperature data. The high heat capacity of water ensures that the reference sections do not change temperature on the timescales measured by the DTS (although they may change temperature over the course of the day, they remain constant during the 1–5 min integration period), and the PT100s provide an independent temperature observation against which the DTS data is calibrated. Using sections of fiber rather than single points improves the accuracy of calibration [Hausner *et al.*, 2011], and the reference sections employed in this study were designed to provide a minimum of 10 observations as recommended by Tyler *et al.* [2009]. To analyze the recorded temperature data, distances on the cable were translated to water depths prior to any statistical or hydrodynamic analysis.

[13] Field campaigns were conducted in January, February, July, and September of 2009. During each deployment, spatially and temporally integrated temperatures were continuously recorded at 1 m integration spatial intervals and 1 or 5 min temporal intervals. The integration times and duration of deployment varied over the course of the four field campaigns (Table 1). To account for these differences, 24 h composite traces were created for each deployment. During a number of these deployments, divers were either present

in the water during monitoring or had been present in the days immediately preceding the deployment. To evaluate the effect of the divers on the temperature profile, the September 2009 campaign included 3 d of continuous monitoring prior to dives, and 24 h of monitoring after the dives began, including 4 h of monitoring with divers in the water.

[14] The Sensonet DTS instrument is provided by the manufacturer with both single-ended and double-ended calibration routines, and the duplexed cable was selected to allow either of these to be used. Single-ended calibration routines assume uniform attenuation of light over the entire length of the optical fiber; double-ended routines allow for spatial variations in attenuation, but assume that light is attenuated at the same rate as it travels in either direction. During installation of the cable, it was damaged in a number of places (Figure 2a), making the manufacturer-provided single-ended routines impossible to use; the assumptions made by these routines introduced steps into the temperature data at the location of each signal loss (Figure 2b). At the same time, an asymmetric signal loss (attenuation that depends on the direction of travel in the fiber) was observed in the MiniBend, preventing the use of the native double-ended calibration routines. Instead, DTS temperatures were calibrated from the raw Raman spectra Stokes and anti-Stokes power ($I_S[z]$ and $I_{aS}[z]$, respectively) using the three-section explicit method described by Hausner *et al.* [2011], based on equation (1),

$$T(z) = \frac{\gamma}{\ln \frac{I_S(z)}{I_{aS}(z)} + C - \Delta\alpha z} \quad (1)$$

In this equation, γ (K) represents the shift in energy between the laser fired by the DTS and the scattered Raman signals observed at the instrument, C is a single parameter that depends primarily on the instrument's photon receptors and the properties of the multimode optical fiber, and $\Delta\alpha$ (m^{-1}) is the differential attenuation between the Stokes and anti-Stokes signals, defined as $\Delta\alpha = \alpha_{aS} - \alpha_S$, where α_{aS} and α_S represent the attenuation rates (m^{-1}) of the anti-Stokes and Stokes signals, respectively. In the three-section explicit method, the values of γ , C , and $\Delta\alpha$ are calculated explicitly for each temporal integration period based on three independently monitored reference sections with at least two different temperatures. The 25 m reference section was divided in two and used as two 10 m reference sections of identical temperatures, and the 15 m in situ reference section was used as the third reference. Using a calibration scheme based on equation (1), Suárez *et al.* [2011] demonstrated a fivefold improvement in root-mean-square error (RMSE) over the manufacturer's calibration routines in a laboratory application, and Hausner *et al.* [2011]

Table 1. Dates and Details of Four 2009 DTS Field Deployments^a

Deployment Dates (All 2009)	Duration (hr)	Integration Time (s)	Frequency (traces d^{-1})	Usable Traces (RMSE ¹ < 0.1°C) ¹ Equation (3)	Total Traces
19–21 January	48	300	288	556	576
17–20 February	72	300	288	844	864
14–16 July	72	60	288	476	576
23–27 September	96	60	1440	5330	5459

^aJuly deployment included collection of data not presented in this paper; although the traces were taken with a 60 s integration time, they were repeated at 5 min intervals.

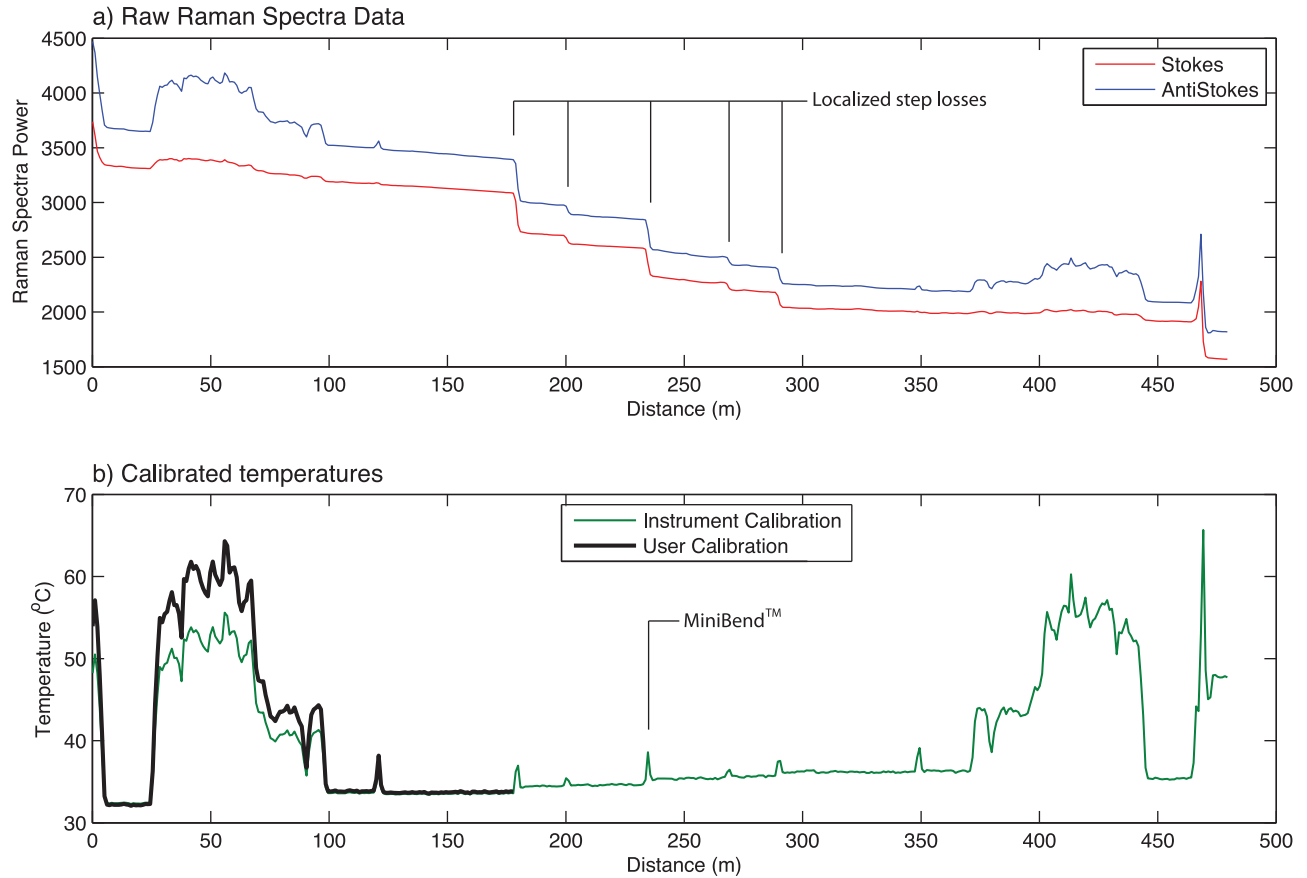


Figure 2. (a) Raw Raman spectra data (presented in arbitrary units linearly related to the power of the observed signals), and (b) instrument calibrated temperatures (green line) and user-calibrated temperatures (black line) record 13:55 PST, 15 July 2009. The signal losses due to the damaged cable are indicated in (a), and the corresponding steps in the instrument-calibrated temperature can be seen in (b). The location of the MiniBend™ (about which the temperatures should be symmetric) is indicated in (b), and the calibration reference sections can be clearly seen in both panels at 8–28 m, 100–115 m, 355–370 m, and 448–468 m. The cable enters the water just after the second reference section, at 123 m.

showed similar improvement in a field study using the three-section explicit calibration method, attaining mean RMSE values on the order of 0.1°C .

[15] Because this calibration method must assume uniform fiber properties [Hausner *et al.*, 2011], the recalibrated data collected in Devils Hole were valid only between the instrument and the first step loss at ~ 178 m (Figure 2a). After calibration, the data were trimmed to omit any locations at which the recorded temperatures were affected by the step losses. As Figure 1 shows, this limits the data to the narrow fracture above the main cavern; this limitation is discussed in more detail in section 3.1 below.

2.3. Composite Temperature Profiles and Statistical Analyses

[16] An RMSE was calculated for each sampling period according to equation (2),

$$\text{RMSE} = \sqrt{\frac{\sum_{i=1}^{n_1} (T_i - T_{\text{ref}_1})^2 + \sum_{i=1}^{n_2} (T_i - T_{\text{ref}_2})^2 + \sum_{i=1}^{n_3} (T_i - T_{\text{ref}_3})^2}{n_1 + n_2 + n_3}}, \quad (2)$$

in which n_1 , n_2 , and n_3 are the number of data points in the three reference sections and T_{ref_1} , T_{ref_2} , and T_{ref_3} ($^{\circ}\text{C}$) are the respective temperatures of the reference sections. During some of the field campaigns, the temperatures in the two reference sections were too similar to yield good calibrations. To avoid these poorly calibrated data, traces with an RMSE value greater than 0.10°C were omitted from the data set, and the remaining traces were combined into 24-h composite mean temperature profiles.

[17] The composite temperature profiles were created by taking the mean of the recorded temperatures at each location over a 24 h period, and the calibrated temperatures were trimmed to reflect only the measurements of deep pool water temperature. The 24-h profiles were compared to one another using the linear Pearson correlation coefficient [Wilks, 2006] to examine the inter- and intraday repeatability, and Spearman's rank correlation [Wilks, 2006] was used as a nonparametric test to determine whether a statistically significant relationship between depth and temperature was observed in each profile. Prior to performing the analyses presented here, the cable distances were translated to water depths by linearly interpolating between three points of known depth: the point at which the cable enters

the water (zero depth), a cable marker read by divers at a depth of 9.8 m, and a second cable marker read at a depth of 23.8 m. The statistics and figures presented in this paper therefore describe relationships between water temperature and water depth.

2.4. Numerical Simulations and Flow Characterization

[18] When statistically significant temperature gradients were observed, the hydrodynamic stability of the temperature profiles was examined using the dimensionless Rayleigh number Ra (equation (3)), which represents the ratio of buoyancy driven heat fluxes to conductive heat fluxes [Bejan, 2004]. For thermal convection processes, the Rayleigh number can be used to distinguish between thermal environments dominated by conduction and those in which convection is the primary driver of heat transfer,

$$Ra = \frac{g\beta\Delta TL^3}{K_T\nu}. \quad (3)$$

In equation (3), g is the acceleration due to gravity (m s^{-2}), β is the three-dimensional thermal expansion coefficient of water (K^{-1}), ΔT (K) is the difference in temperature between the top and bottom of the fluid volume, L is a length scale, K_T is the thermal diffusivity of the fluid ($\text{m}^2 \text{s}^{-1}$), and ν ($\text{m}^2 \text{s}^{-1}$) is the kinematic viscosity of the fluid [Bejan, 2004]. In an infinitely wide, free-fluid system with a constant temperature difference between the top and bottom, stability analysis predicts the onset of laminar convection when the Rayleigh number exceeds 1708, and turbulent convection at Rayleigh numbers greater than 10^7 [Bejan, 2004]. For each composite temperature profile that exhibited a statistically significant temperature gradient, the Rayleigh number was calculated using equation (3). In this calculation, the value of ΔT was calculated using a linear regression of temperature with depth as the difference between the shallowest and deepest point on the regression line, and the length scale used was the depth of the deepest observation (~ 34 m).

[19] To better understand the apparently unstable gradients observed, numerical simulations of thermal convection in a two-dimensional analog to Devils Hole were made using FLUENT (ANSYS, Inc., Canonsburg, Pennsylvania), a computational fluid dynamics (CFD) package capable of simultaneously modeling heat, mass, and solute transfer in fluid systems. The simulations were designed to examine the potential influence of the fracture walls and the surrounding thermal gradient on convection in the system, and necessarily reflected an extremely simplified geometry rather than the full complexity of the natural system. The deep pool of Devils Hole was modeled as a 10 m deep by 50 cm wide column of water, slanted at an angle of 22° from vertical to match the angle shown in Figure 1b, and water temperatures at the model boundaries were scaled according to Rayleigh number. A 10 m column of water was sufficiently deep to keep water temperatures and temperature-dependent properties within a realistic range (25°C – 39°C), but small enough to allow efficient simulation on the available computers. No-flow boundaries were defined on all four sides of the column, and the column was discretized into 2.5 cm quadrilateral cells. Constant temperatures were

defined at the top and bottom of the column, and constant sidewall temperatures were fixed on a linear gradient between the surface and bottom temperatures. Second order approximations were used to simultaneously solve equations for conservation of energy, conservation of momentum, and conservation of mass.

[20] Two different conditions were simulated, modeling the thermal regimes observed in both summer and winter conditions. Under summer conditions, top and bottom temperatures were 33.35°C and 39.15°C , respectively, to induce a simulated Rayleigh number of 10^{14} . The winter simulation held the bottom temperature constant at 39.15°C and decreased the top temperature to 24.45°C , doubling the simulated Rayleigh number; this difference scales to a drop of $\sim 0.2^\circ\text{C}$ at the surface of Devils Hole. Initial water column temperatures were set to match the gradients in the sidewalls, and both scenarios were run as transient simulations. To allow the model to adapt to the initial condition without becoming unstable, a variable time step was used with an initial step of 0.001 s. After the immediate response to the initial condition was stabilized, the model quickly progressed to the maximum time step of 15 s. Each simulation was run for 46 d. The first 24 h were set aside to establish quasi-steady state conditions, and water temperatures and velocities were then recorded on 24 h intervals beginning at $t = 48$ h. Under each scenario, 45 temperature profiles were recorded along the slanted centerline of the column, while vertical water velocities were recorded throughout the entire column at the same time. A Reynolds number (equation (4)), representing the ratio of inertial forces to viscous forces [Roberson and Crowe, 1993], was calculated for each of the 45 “snapshots,”

$$Re = \frac{\rho VL}{\mu}. \quad (4)$$

In equation (4), ρ represents the fluid density, μ represents the dynamic viscosity of the fluid, V represents a characteristic velocity of the system, and L is a characteristic length scale. In the CFD simulations, the characteristic length scale was twice the width of the column, to reflect flow in a wide duct [Roberson and Crowe, 1993]. The density and viscosity were calculated based on the mean temperature of the water column, and the velocity used was the maximum vertical velocity simulated in the entire column. The Reynolds number can be considered an indicator of the impact of viscous forces; flows with Reynolds numbers less than 50,000 experience significant viscous forces, while flows at higher Reynolds numbers tend to be dominated by inertial forces [Roberson and Crowe, 1993].

3. Results and Discussion

3.1. DTS Temperature Profiles

[21] The 11 24-h temperature profiles are shown in Figure 3, and details of each profile (including the strength of the raw Raman signals, any statistically significant thermal gradient, and the Rayleigh number for significant gradients) are provided in Table 2. Figure 4 shows the mean temperature profiles from the winter and summer observations on a single plot, and Table 3 contains the statistical

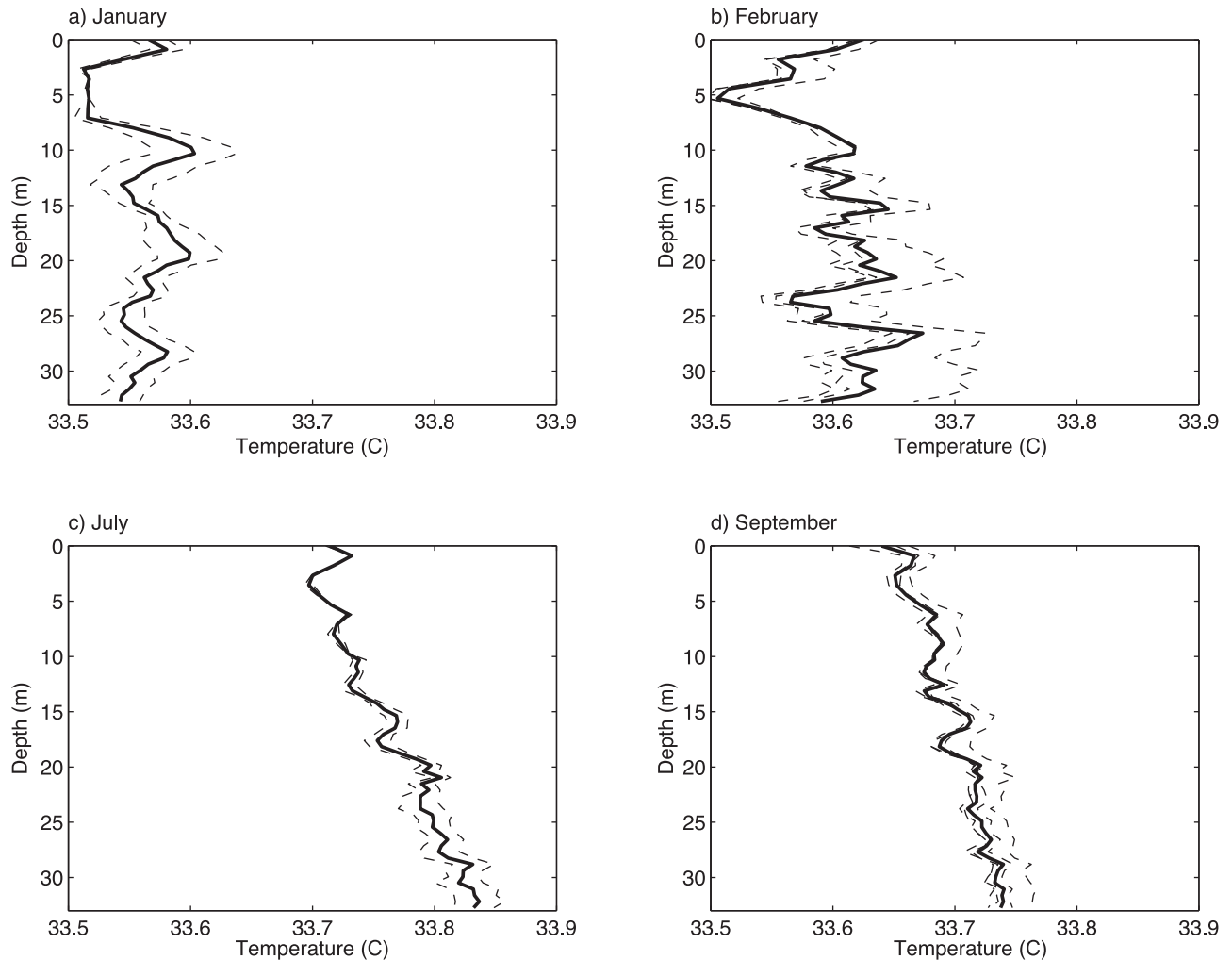


Figure 3. Twenty-four-hour temperature profiles (fine dashed lines) and mean temperature profiles (heavy black lines) recorded during the four 2009 field campaigns. (a) January, (b) February, (c) July, and (d) September.

comparisons between the four composite profiles. The profiles were generated from raw Raman data of similar intensity (Table 3) calibrated using the same methods and reference instruments. The deviations from the mean (Figure 5) do not appear to be cyclical or correlated to earth tides or diurnal

temperature signals. These data clearly show statistically significant ($\alpha < 0.05$) thermal gradients in July and September and less depth-dependent temperatures in the winter months. The January data show a near-uniform temperature with depth, indicating convective mixing processes that distributed

Table 2. Details of Each 24-h Composite Temperature Profile^a

Profile	Start Date and Time (PST)	Reference Stokes Power ($\mu \pm \sigma$)	Spearman's ρ	Pearson's R	Linear Temperature Gradient ($^{\circ}\text{C m}^{-1}$)	Rayleigh Number
1	19 January 9:58	3293 ± 341	0.084	0.145	–	–
2	20 January 9:58	3010 ± 244	0.029	0.187	–	–
3	17 February 14:36	3172 ± 319	0.79	0.779	–	–
4	18 February 14:36	3021 ± 301	0.305	0.424	–	–
5	19 February 14:36	3091 ± 274	0.213	0.308	–	–
6	14 July 15:06	3168 ± 262	0.956	0.952	0.0037	8.0×10^{13}
7	15 July 15:06	3344 ± 266	0.979	0.975	0.0049	1.1×10^{14}
8	23 September 11:23	2554 ± 219	0.937	0.929	–	–
9	24 September 11:23	2516 ± 200	0.966	0.958	0.0029	6.2×10^{13}
10	25 September 11:23	2570 ± 210	0.923	0.931	–	–
11	26 September 11:23	2624 ± 229	0.955	0.954	0.003	6.5×10^{13}

^aReference Stokes power is the mean power of the temperature independent Raman Stokes signal observed in the in situ reference coil. Statistical analyses include Spearman's rank correlation (a nonparametric test for significance) and Pearson's correlation coefficient (a test for linear correlation). In the case of a statistically significant relationship ($P < 0.05$), the linear temperature gradient ($^{\circ}\text{C m}^{-1}$ water depth) and Rayleigh numbers are also presented.

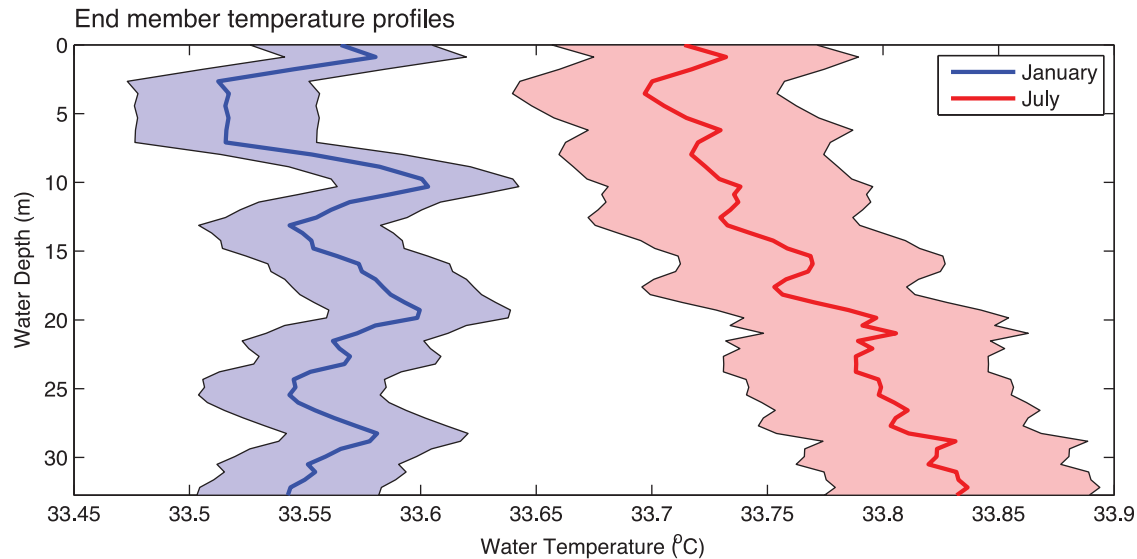


Figure 4. Summer and winter temperature profiles observed during the course of 2009. The shaded areas indicate the mean temperature plus/minus the RMSE of the user-calibrated temperature data.

heat uniformly throughout the profile. The February data appear to represent a transition between the uniform January temperature profile (convective mixing) and the stratified temperature profiles in July and September, and the statistical comparisons of the profiles bear this out. Pearson's correlation coefficient (R) between the January and February profiles is 0.54, while the February–July and February–September correlation coefficients are both 0.57. The July and September profiles are highly correlated with each other ($R = 0.96$). These correlations point toward a seasonal pattern of convective mixing and thermal stratification in Devils Hole.

[22] Water temperatures on the shallow shelf of Devils Hole exhibit a high seasonal variability when compared to the rest of the system. While the water temperatures in the deep pool remain within a few tenths of a degree of the mean, the temperatures on the shallow shelf vary up to 4°C with the changes in ambient air temperature and direct solar insolation over the year [Threlloff and Manning, 2003]. During the winter, cooler water runs off the shelf into the deeper pool, mixing with the warmer water below it and resulting in the near-uniform temperature profile observed in January. In the summer and early fall, the water on the shelf is warmer, and the density difference between the shallow shelf water and the deep water is not sufficient to cause such convective mixing. The mean surface temperature of the deep pool in January 2009 was 33.17°C ; in July, the mean surface temperature was 0.24°C greater at 33.41°C .

[23] It is important to note the limitations of the data collected in the field. As mentioned earlier, the observed

temperature profiles are limited to the water column above the large cavern, and the numerical model was intended to simulate only this area. From an ecological perspective, this is the part of the system that is critical to the pupfish population; the majority of individuals are found in the top 10 m of the water column, and pupfish are seldom observed below Anvil Rock (~ 23 m below the water surface). The hydrodynamics at the constriction pose an interesting question, but data presented here are insufficient to examine that issue.

3.2. Numerical Simulations of Mixing Process

[24] The stratified temperature profiles observed in July and September are atypical of lake or other surface water systems; instead, the inverted profiles more closely resemble near-surface geothermal gradients, and are similar to other profiles observed in the carbonate aquifer of the Death Valley regional flow system [Reiner, 2007]. The Rayleigh numbers calculated from the July and September temperature profiles are on the order of 10^{13} – 10^{14} , well in excess of both the threshold that indicates the onset of thermally driven convective mixing ($Ra > 1708$) and also the 10^7 threshold that predicts turbulent mixing [Bejan, 2004]. However, the Rayleigh number as an indicator of convection is based on a thermal perturbation applied at the top and bottom of an infinitely wide column of water, with no horizontal heat transfer. The geometry of Devils Hole is clearly at odds with these assumptions, and the limestone walls also provide system boundaries that allow heat to transfer between the substrate and the water column. Borehole data from wells in the carbonate aquifer of the Ash Meadows subbasin of the Death Valley regional flow system show strong linear temperature gradients [Reiner, 2007]. If the walls of Devils Hole show a similar temperature gradient, then heat transfer between the water column and the walls can and will occur.

[25] The results of the summer and winter numerical simulations (Table 4 and Figure 6) show the same patterns observed in the field. The summer simulations, based on

Table 3. Pearson's Linear Correlation Matrix for the Mean Temperature Profiles From the Four 2009 Deployments

January	February	July	September	
1	0.546	0.219	0.210	January
	1	0.562	0.542	February
		1	0.963	July
			1	September

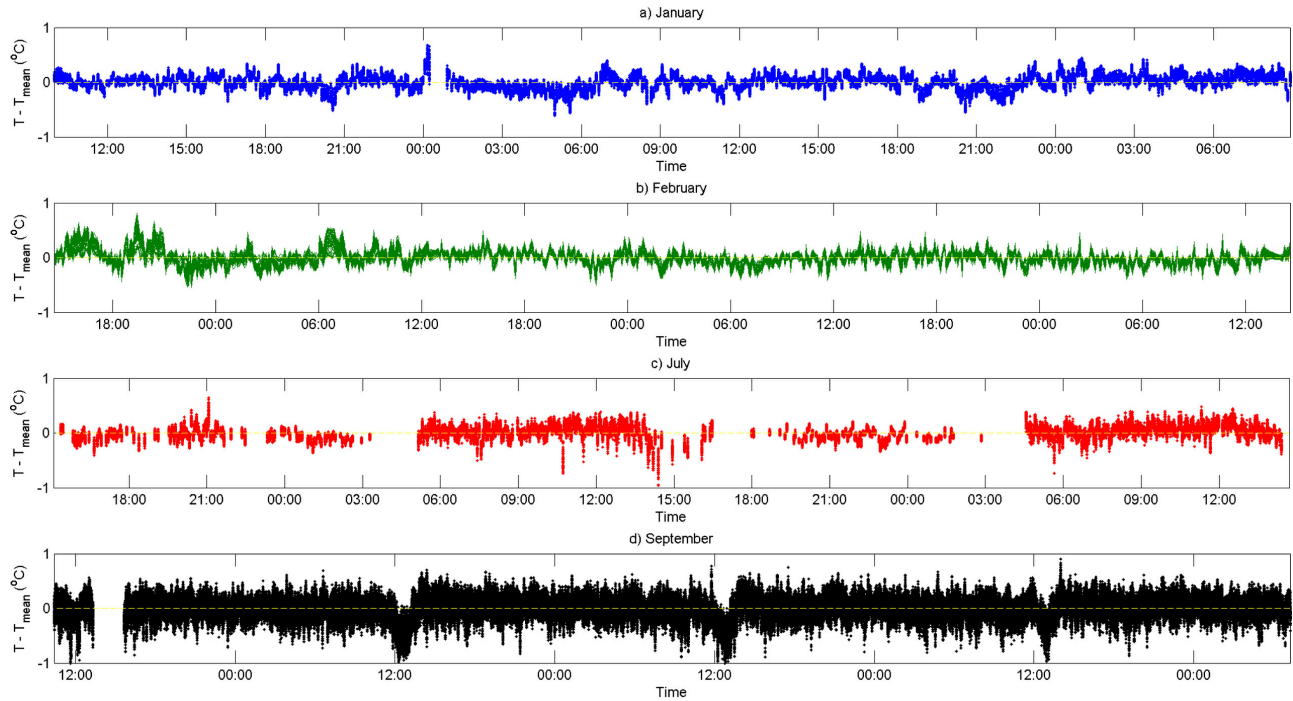


Figure 5. Deviations from the mean temperature in time for the (a) January, (b) February, (c) July, and (d) September field campaigns.

the temperature gradient of $0.005^{\circ}\text{C m}^{-1}$ observed in July, result in a constant, statistically significant temperature gradient within the model. For every one of the 45 recorded temperature profiles, Spearman's ρ for temperature versus depth was 0.98, and the simulated temperature gradient in those 45 profiles was $0.406 \pm 0.0002^{\circ}\text{C m}^{-1}$ (mean \pm standard deviation of the 45 measurements). Reynolds numbers for the summer simulations range from 2.8 to 3.4×10^4 , with a mean and standard deviation of $3.1 \pm 0.2 \times 10^5$. Reynolds numbers in this magnitude range indicate a significant influence of drag forces on water flows, and are consistent with a stable, stratified temperature profile.

[26] The winter simulations are very different. A slight temperature gradient is still apparent, although the winter gradient is not statistically significant (the maximum Spearman's ρ observed for temperature versus depth was 0.88). The gradient, however, is an order of magnitude less and more variable than the summer gradient: the simulated winter temperature gradient is $0.028 \pm 0.004^{\circ}\text{C m}^{-1}$

(mean \pm standard deviation of 45 profiles). Reynolds numbers for the winter simulations reflected the less stable gradients, ranging from 0.7 to 1.1×10^5 , with a mean and standard deviation of $8.5 \pm 0.9 \times 10^4$.

[27] The stark differences between the summer and winter simulations support the feasibility of changing convection patterns driven by variations in surface temperature and resisted by heat transfer from the walls of the system. With the summer and winter Reynolds numbers on opposite sides of the threshold between viscous and inertial flow, the Reynolds number in particular points toward a fundamental shift in the simulated flow regime between the two seasons. This simulated shift is driven by boundary condition changes analogous to the difference between the January and July shallow shelf temperatures. Scaling the simulated Rayleigh numbers to the dimensions of Devils Hole indicates that very small temperature changes at the water surface could result in meaningful changes in circulation at depths above the main cavern. Despite the low ratio of surface area to volume, the simulated mixing phenomena appear to be feasible.

[28] Persistent perturbations in the summer temperature profiles also point toward a stable water column. Consider the local deviations seen between 12 and 17 m in the July and September temperature profiles (Figures 3c and 3d). An examination of the raw data on which these temperatures are based indicates that these deviations are real phenomena: the Raman spectra signals are attenuated in a way that indicates real temperature changes rather than artifacts of physical strains or stresses on the fiber. The normal (uniform temperature) attenuation rates of the Raman Stokes and anti-Stokes signals in the fiber are ~ 2.5 and 2.7 dB km^{-1} , respectively. In September, however, the mean attenuation

Table 4. Numerical Simulation Results^a

Feature	Summer Simulation	Winter Simulation
Statistically significant temperature gradient	$0.406 \pm 0.0002^{\circ}\text{C m}^{-1}$	N/A
Spearman's Rho	0.979 ± 0.000	N/A
Nonstatistically significant temperature gradient	N/A	$0.02 \pm 0.003^{\circ}\text{C m}^{-1}$
Coefficient of determination (R^2) between depth and temperature	0.96 ± 0.00	0.68 ± 0.07
Reynolds number	$31,000 \pm 1800$	$85,000 \pm 8600$

^aData are reported as mean \pm SD of 45 simulated profiles.

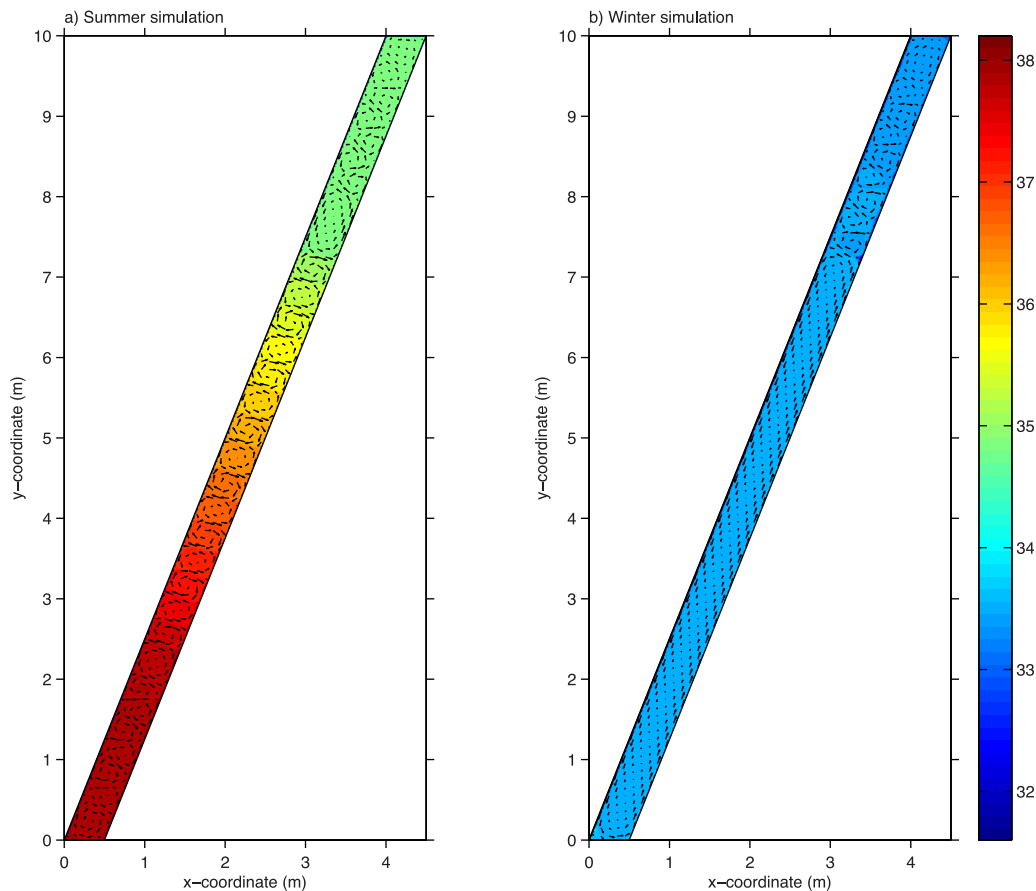


Figure 6. Typical simulated water column temperatures ($^{\circ}\text{C}$, indicated by color) and convection patterns (indicated by directional arrows). (a) Summer simulation and (b) winter simulation. Water temperatures are plotted at the grid resolution of 2.5 cm. For clarity, velocity vectors are plotted at 5 cm resolution.

rates of these signals between 12 and 15 m are 1.2 and 1.6 dB km^{-1} , respectively; between 15 and 17 m the attenuation rates approach the baseline rate of 2.3 and 2.4 dB km^{-1} , respectively. The Raman spectra data for July exhibit a similar pattern. While attenuation rates can increase as a result of strains in the fiber, apparent reductions in the attenuation rate can be attributed only to temperature changes. These localized areas of elevated temperature may be due to horizontal flux of warmer water or to contact between the fiberoptic cable and warmer cavern walls, but either phenomenon represents a conductive heat flux within the system. The localized anomalies are not present during the January and February profiles, when such conductive fluxes would be overwhelmed by the vertical convective heat fluxes within the system.

3.3. Effects of Divers on Vertical Mixing Processes

[29] Data collected during the September deployment provide the opportunity to examine the effects of divers on the temperature profiles. If the presence of divers in the water were to disrupt the stable profile, this disturbance should be evident from comparing the temperatures recorded before, during, and immediately after the dives. This would be especially important during the July and September deployments; any perturbations caused by the

divers would disrupt the stable temperature profiles that were observed during these periods. The first 72 h of the September deployment were recorded without divers in the water; four divers entered the water at 08:38 PST, 26 September 2009, while the DTS continued to collect data for 24 h after the first dive. Three dives were undertaken on 26 September (08:38–09:28, 11:11–11:58, and 13:35–14:24), and a fourth dive (07:56–08:46) was included in the temperature record on 27 September. The DTS deployment was terminated during the fifth dive, which began 27 September at 10:05. The temperature profiles, however, appeared to be undisturbed; the data recorded during and after the September dives continued to exhibit the same temperature gradient as the pre-dive data did, and the points at which the divers entered or exited the water are indistinguishable from the pre-dive temperature profile.

[30] Data recorded during the July deployment, which occurred immediately following a series of 12 dives over 3 d, support this as well. Despite the repeated dives, a statistically significant temperature gradient was observed each day of the July deployment. In this case, the temperature gradient appears to be slightly greater on the second day of the deployment ($\nabla T = 0.0049^{\circ}\text{C m}^{-1}$, compared to $0.0037^{\circ}\text{C m}^{-1}$ on the first day), and the temperature profile likewise appears to be more strongly related to depth on the

second day of data collection than on the first (Spearman's $\rho = 0.979$, compared to 0.956 on the first day). While this may indicate a slight disturbance to the temperature profile as a result of repeated dives, it was not repeated in the September data. It is worth noting that the series of dives in July included an unprecedented amount of work: three dives a day were conducted over the 72 h prior to the collection of DTS data, and the divers occasionally placed a net (which had not previously been used) across the edge of the shelf for an hour at a time. It is likely that the July dives resulted in a greater disturbance than the September dives did, especially in the transition zone between the shallow shelf and the deep pool; however, the overall disturbance was not sufficient to disrupt the constant temperature profile observed in the deep pool.

[31] In the September data set, there do not appear to be any disturbances in the temperature profile that can be attributed to the activity of the divers. A number of researchers, policy makers, and other stakeholders have questioned the impacts of repeated diving in Devils Hole. These data indicate that repeated, active dives may slightly disrupt the temperature profile of the system, but they neither significantly encourage nor inhibit the natural convective processes that control the circulation of water within the upper portion of the deep pool. The presence of four divers in the water and the associated mixing is not sufficient to disrupt the temperature profile, while small temperature changes at the water surface are. Data on the physical habitat of Devils Hole collected by divers and instrumentation during the regularly scheduled dives appear to be representative of the state of the system.

3.4. Ecological Impacts of Seasonal Convective Mixing

[32] Convective mixing plays a significant role in the ecosystems of many temperate lakes, and its role in a resource-limited setting like Devils Hole is likely critical to the geochemistry and energetics of the system. Devils Hole is a unique system in that the depth of the bottom is unknown. In most temperate lakes, convective mixing will bring anoxic water, anaerobic sediments and organisms, and settled detritus up from the bottom of the system to mix with the oxygenated water near the surface; the fast changes in redox state and temperature spur chemical and biological processes that control the ecology of the lake (the oxidation and dissolution of reduced phosphorus species may increase the available nutrients in the water column, for example). In the groundwater-dominated setting of Devils Hole, however, this does not occur. The ultraoligotrophic deep water of Devils Hole contains very little organic material that may be utilized by the pupfish as a food source [D. P. Moser, Desert Res. Inst., personal communication, 2010]. Rather than bringing up anoxic water and reduced sediments to be oxidized, the water displaced from the depths of Devils Hole contains primarily dissolved calcium carbonate, although nutrient concentrations above background levels have been observed after occasional surface runoff events.

[33] The seasonal nature of the mixing processes observed at Devils Hole is especially important to the pupfish population because the timing of the mixing coincides with periods of little available light and low primary productivity. While Devils Hole pupfish are sometimes observed as deep as

26 m, a majority of the observed pupfish are found on the shelf during the spring and fall seasons. In summer and winter, the fish appear to migrate to the waters of the adjoining deeper pool [Baugh and Deacon, 1983] although most fish are found in the top 5 m of the water column throughout the year. During these times, the pupfish diet is strongly dependent on allochthonous carbon sources [Wilson and Blinn, 2007]. Any allochthonous material deposited on the water surface may not remain there; when the water on the surface cools, this material will be carried down to the depths of Devils Hole and replaced by deeper water that does not contain the same concentrations of available carbon or nutrients. This is especially true for dissolved nutrients and smaller particulate material suspended in the water column; larger plant matter can persist on the shelf for months. The *S. calida* that comprises more than 50% of the pupfish's winter diet subsists on allochthonous submerged plants during the winter [Wilson and Blinn, 2007]. While Wilson and Blinn [2007] measured allochthonous carbon inputs, those observations may have underestimated the fraction of those inputs that remain available to *S. calida*, and thus to the pupfish population, in the winter months.

[34] Because mixing appears to be driven by falling water temperatures on the shallow shelf, anything that encourages lower water temperatures on the shelf could impact the pupfish population. The timing of the seasonal mixing will depend on not only air temperature, but also on the water level on the shelf. It was noted above that water temperatures can drop to as low as 30°C when nighttime low temperatures coincide with low tide periods [Threlhoff and Manning, 2003]; if the water level (and the corresponding thermal mass) on the shelf were to decrease, it may be possible for deep convection cells to establish overnight, even during summer. By sweeping the near-surface nutrients, both allochthonous and autochthonous, to the depths of Devils Hole, convective cells could reduce the availability of food in the ecosystem; such a reduction in a system that is already food-limited could be disastrous for the pupfish population. Although cooler water temperatures on the shallow shelf encourage spawning activity and successful hatches, the mixing induced by the winter temperature provides a negative feedback by removing food from the shallow habitat.

[35] At the same time, the seasonal mixing cycles offer a positive feedback for spawning in areas below the shallow shelf. While spawning behavior has been observed as deep as 27 m, larvae are seldom seen in the deeper habitat. Winter mixing has the potential to cool the water at these depths, encouraging successful spawning, while simultaneously delivering nutrients to the larvae that may hatch in the deeper parts of the system. With hydrodynamic modeling and CFD simulations, it may be possible to link Ash Meadows air temperatures and other environmental drivers to the onset of vertical mixing. If this can be accomplished, then comparing historic meteorological records to annual estimates of winter pupfish mortality may offer a potential explanation for the recent decline of the *C. diabolis* population in Devils Hole.

4. Conclusions

[36] The waters of Devils Hole appear to exhibit a seasonal pattern of vertical mixing and stabilization driven by the combination of air temperatures and geothermal

temperature gradients. The geothermal influence causes the temperature profile of Devils Hole to be inverted when compared to typical temperate limnological profiles. The stable summer gradient is influenced not only by the walls of the fracture, but also by horizontal groundwater flows through discrete zones of high permeability. While the conditions that drive this convection are described qualitatively in this paper, further quantitative work and CFD modeling may make it possible to link the vertical mixing processes to environmental thresholds (water level and ambient air temperature, for example) that result in the onset or cessation of thermal convection.

[37] The convective mixing observed during the winter months may have significant impacts on the pupfish population, especially considering the resource-limited nature of the system and the dependence of the pupfish population on allochthonous carbon inputs during periods of low primary productivity. Because of this dependence, the timing of the mixing phenomena observed here is critical. Reductions in the water surface elevation could exacerbate this impact by increasing the threshold air temperature that results in the onset of this convection, leading to the onset of convective mixing earlier in the year. With additional monitoring and CFD simulations, it may be feasible to predict impacts of climate change, changes in the mean water level of Devils Hole, and various other environmental drivers on the thermal regime and convective setting of Devils Hole. Such knowledge would be an invaluable tool, both for understanding the physical processes at work in the ecosystem and for management considerations for Devils Hole. Further investigation of convection in this ecosystem is certainly warranted, especially in light of the precarious position of the Devils Hole pupfish population.

[38] From a larger perspective, the high-resolution spatial and temporal temperature observations and precise calibration made possible by fiber-optic DTS systems have allowed us to observe and quantify extremely fine temperature gradients, and numerical simulations support the high-precision temperature observations. Precisely calibrated temperature observations on the spatial and temporal scales made possible by DTS instruments can reveal phenomena that were previously lost in instrument noise and measurement uncertainties.

[39] **Acknowledgments.** The authors greatly appreciate the thoughtful and constructive comments of Barry Freifeld, Jim Constantz, and two anonymous reviewers, whose comments significantly improved and clarified the manuscript. We gratefully acknowledge funding from the United States National Park Service, Nevada Department of Wildlife, and the Death Valley Natural History Association. We thank Michael Bower, Michael Young, Tony Berendsen, Christine Hatch, and the Devils Hole Dive Team for their help in preparing and installing equipment in the field, as well as Gayton Scoppettone, Duane Moser, Paul Barrett, and Francisco Suarez for their suggestions and guidance.

References

- Andersen, M. E., and J. E. Deacon (2001), Population size of Devils Hole pupfish (*Cyprinodon diabolis*) correlates with water level, *Copeia*, 2001(1), 224–228.
- Anderson, M. P. (2005), Heat as a ground water tracer, *Ground Water*, 43(6), 951–968, doi:10.1111/j.1745-6584.2005.00052.x
- Baugh, T. M., and J. E. Deacon (1983), Daily and yearly movement of the Devils Hole pupfish (*Cyprinodon diabolis*) Wales in Devils Hole, Nevada, *Great Basin Nat.*, 43(4), 592–596.
- Bear, J., and A. H.-D. Cheng (2010), *Modeling Groundwater Flow and Contaminant Transport*, 850 pp., Springer Science and Business Media, N. Y.
- Bejan, A. (2003), Porous media, in *Heat Transfer Handbook*, edited by A. Bejan and A. D. Krause, pp. 1131–1180, John Wiley, Hoboken, N. J.
- Bejan, A. (2004), *Convection Heat Transfer*, 3rd ed., 694 pp., John Wiley, Hoboken, N. J.
- Chernoff, B. (1985), Population dynamics of the Devils Hole pupfish, *Environ. Biol. Fish.*, 13(2), 139–147, doi:10.1007/BF00002582.
- Faunt, C. C., F. A. D'Agnesi, and G. M. O'Brien (2004), Hydrology, in Death Valley Regional ground-water flow system, Nevada and California—hydrogeologic framework and transient ground-water flow model, edited by W. R. Belcher, *U. S. Geol. Surv. Sci. Invest. Rep. 2004-5205*, pp. 137–163.
- Hausner, M. B., F. Suárez, K. E. Glander, N. C. van de Giesen, J. S. Selker, and S. W. Tyler (2011), Calibrating single-ended fiber-optic Raman spectra distributed temperature sensing data, *Sensors*, 11, 10,859–10,879, doi:10.3390/s111110859.
- Lema, S. C., and G. A. Nevitt (2006), Testing an ecophysiological mechanism of morphological plasticity in pupfish and its relevance to conservation efforts for endangered Devils Hole pupfish, *J. Exp. Biol.*, 209(18), 3499–3509, doi:10.1242/jeb.02417.
- Meffe, G. K. (1986), Conservation genetics and the management of endangered fishes, *Fisheries*, 11(1), 14–23, doi:10.1577/1548-8446(1986)0112.0.CO;2.
- Miller, R. R. (1950), Speciation in fishes of the genera *Cyprinodon* and *Empetrichthys* inhabiting the Death Valley region, *Evolution*, 4(2), 155–163.
- Reiner, S. R. (2007), Groundwater temperature data, Nevada Test Site and vicinity, Nye, Clark, and Lincoln counties, Nevada, 2000–2006, *U. S. Geol. Surv. Data Series 269*, 20 pp.
- Riggs, A. C., and J. E. Deacon (2002), Connectivity in desert aquatic ecosystems: The Devils Hole Story, paper presented at Spring-fed Wetlands: Important Scientific and Cultural Resources of the Intermountain Region, May 7–9, 2002, Las Vegas, Nev., DHS Publication 41210, Retrieved (January 2009) from Desert Research Institute web site, available at <http://wetlands.dri.edu>.
- Roberson, J. A., and C. T. Crowe (1993), *Engineering Fluid Mechanics*, 5th ed., 785 pp., Houghton Mifflin, Boston, Mass.
- Selker, J. S., N. C. van de Giesen, M. Westhoff, W. Luxemburg, and M. Parlange (2006), Fiber-optics opens window on stream dynamics, *Geophys. Res. Lett.*, 33, L24401, doi:10.1029/2006GL027979.
- Suárez, F., S. W. Tyler, and A. E. Childress (2010), A fully coupled, transient double-diffusive convective model for salt-gradient solar ponds, *Int. J. Heat Mass Transfer*, 53(9–10), 1718–1730, doi:10.1016/j.ijheatmasstransfer.2010.01.017.
- Suárez, F., J. E. Aravena, M. B. Hausner, A. E. Childress, and S. W. Tyler (2011), Assessment of a vertical high-resolution distributed-temperature-sensing system in a shallow thermohaline environment, *Hydrol. Earth Syst. Sci.*, 15(3), 1081–1093, doi:10.5194/hess-15-1081-2011.
- Szabo, B. J., P. T. Kolesar, A. C. Riggs, I. J. Winograd, and K. R. Ludwig (1994), Paleoclimatic inferences from a 120,000-yr calcite record of water-table fluctuation in Browns Room of Devils Hole, Nevada, *Quat. Res.*, 41(1), 59–69, doi:10.1006/qres.1994.1007.
- Threlloff, D., and L. Manning (2003), Thermal environment of the Devils Hole pupfish (*Cyprinodon diabolis*), draft rep., 29 pp., Death Valley National Park, Furnace Creek, Calif.
- Tyler, S. W., J. S. Selker, M. B. Hausner, C. E. Hatch, T. Torgersen, C. E. Thodal, and S. G. Schladow (2009), Environmental temperature sensing using Raman spectra DTS fiber-optic methods, *Water Resour. Res.*, 45, W00D23, doi:10.1029/2008WR007052.
- Wilks, D. S. (2006), *Statistical Methods in Atmospheric Sciences*, 4th ed., 627 pp., Academic, San Diego, Calif.
- Wilson, K. P., and D. W. Blinn (2007), Food web structure, energetics, and importance of allochthonous carbon in a desert cavernous limnocene: Devils Hole, Nevada, *West. N. Am. Naturalist*, 67(2), 185–198, doi:10.3398/1527-0904(2007)67[185:FWSEAI]2.0.CO;2.
- Winograd, I. J., J. M. Landwehr, T. B. Coplen, W. D. Sharp, A. C. Riggs, K. R. Ludwig, and P. T. Kolesar (2006), Devils Hole, Nevada delta O-18 record extended to the mid-Holocene. *Quat. Res.*, 66(2), 202–212, doi:10.1016/j.yqres.2006.06.003.

D. B. Gaines and K. P. Wilson, Resource Management Div., Death Valley National Park, 1321 S. Hwy. 160, Pahrump, NV 89048, USA.

M. B. Hausner and S. W. Tyler, Department of Geologic Sciences and Engineering, University of Nevada, Reno, MS 172, Reno, NV 89557, USA. (mhausner@unr.edu)